

Modelling synchrotron and synchrotron self-Compton emission of gamma-ray burst afterglows from radio to very-high energies

Jagdish C. Joshi^{1,2,3} * and Soebur Razzaque¹ †

¹Centre for Astro-Particle Physics (CAPP) and Department of Physics, University of Johannesburg, PO Box 524, Auckland Park 2006, South Africa

²School of Astronomy and Space Science, Nanjing University, Nanjing 210093, China

³Key laboratory of Modern Astronomy and Astrophysics (Nanjing University), Ministry of Education, Nanjing 210093, China

6 November 2019

ABSTRACT

Synchrotron radiation from a decelerating blast-wave is a widely accepted model of optical to X-ray afterglow emission from gamma-ray bursts (GRBs). GeV gamma-ray emission detected by the Fermi Large Area Telescope (LAT) and the duration of which extends beyond the prompt gamma-ray emission phase, is also compatible with broad features of afterglow emission. There is, however, limitations of the simplest version of this pure electron-synchrotron model to explain high-energy photons detected late from the GRB as well as multiwavelength spectral and temporal features. We have developed a synchrotron self-Compton (SSC) emission model from a decelerating blast-wave and applied it, together with the synchrotron emission model, to fit multiwavelength data from a few bright GRBs detected by the Fermi-LAT. We have explored and derived constraints on the SSC model parameters from fits to the broadband spectra and light curves for the fast- and slow-cooling regimes of electrons in the blast-wave. The results are presented for the long GRB 130427A and short GRB 090510, together with predicted flux in the very-high energy (VHE, $\gtrsim 30$ GeV) range for the current and upcoming ground-based Cherenkov telescopes.

Key words: Gamma-Ray Bursts : GeV-TeV Component, Multi-Wavelength Emission

1 INTRODUCTION

The afterglow emission from GRBs was predicted in radio, optical and X-rays by Paczynski & Rhoads (1993); Mészáros & Rees (1997); Vietri (1997). These predictions were followed by the discovery in 1997, with X-ray and optical afterglow observations from the GRB 970228 (Costa et al. 1997; van Paradijs et al. 1997). Most of the afterglow radiation features are explained using synchrotron model by Panaitescu & Mészáros (1999); Sari et al. (1998); Chevalier & Li (2000); Granot & Sari (2002). More recently the synchrotron models have been successful to interpret Fermi-LAT observations of late GeV emission from GRBs (Kumar & Barniol Duran 2009; Ghisellini et al. 2010; Razzaque et al. 2010); see also Gehrels & Razzaque (2013) for reviews of GeV emission.

The intensity of the self-Compton signals from the blast-waves when they interact with the circumburst medium, was predicted by Meszaros & Rees (1994). More detailed calculations were carried out later on by Chiang & Dermer (1999) and by Zhang & Mészáros (2001). Sari & Esin (2001) also calculated the SSC component when the GRB blast-wave is adiabatic and it ex-

pands into the circumburst medium. This component can contribute significantly to the delayed GeV component in GRB afterglows (Liu et al. 2013; Panaitescu et al. 2013; Wang et al. 2019). These observations are very promising for current and upcoming ground-based Cherenkov telescopes for transients due to higher sensitivity in GeV-TeV energy band. In fact, the MAGIC and HESS have recently announced detection of TeV emission from GRB 190114C (Mirzoyan et al. 2019) and GRB 180720B (Piel et al. 2019). More recently, HESS detected TeV emission from GRB 190829A with high significance (de Naurois 2019). These detections have renewed modelling activities of these bursts (see, e.g., Fraija et al. 2019a; Derishev & Piran 2019; Fraija et al. 2019b; Ronchi et al. 2019; Fraija et al. 2019c; Ajello et al. 2019).

Afterglow observations are important to estimate the shock-energy distribution in electrons ϵ_e , protons ϵ_p and in the magnetic field ϵ_B . These observations also help us to constrain the particle acceleration, jet features, time evolution of the blast-wave as well as the circumburst medium density. The power-law electron energy distribution to model the GRB afterglows can have a broad spectral-index in the range of 1.4-2.8 as found in a set of GRBs by Panaitescu & Kumar (2001). In their set of GRBs the circumburst medium density needed was in the range 0.1-50 cm^{-3} and for GRB 990123 it could go lower than 0.01 cm^{-3} . A similar value of 0.03 cm^{-3} of circumburst medium density was

* jjoshi@nuj.edu.cn
† srazzaque@uj.ac.za

found in GRB 970508 using afterglow synchrotron emission model (Wijers & Galama 1999). For the detectability of an SSC component in the afterglow, a higher density; greater than 1 cm^{-3} ; has been estimated by Sari & Esin (2001). In the wind-type progenitors, 1000 km s^{-1} wind velocity and a wind mass-loss rate of $3 \times 10^{-6} M_{\odot} \text{ yr}^{-1}$ was reported by Chevalier & Li (2000). Similar wind speeds with very low mass loss rate $4 \times 10^{-8} M_{\odot} \text{ yr}^{-1}$ was found for GRB 130427A (Panaitescu et al. 2013). Long GRB 130427A afterglow emission can also be modelled in a constant-density medium using a density 6 cm^{-3} (Liu et al. 2013) and also using a lower density of $2 \times 10^{-3} \text{ cm}^{-3}$ (Panaitescu et al. 2013). For GRB 090510, a two component model by Corsi et al. (2010) needs very low density of 10^{-6} cm^{-3} in the circumburst environment while the proton synchrotron model by Razzaque (2010) requires a constant density of 3 cm^{-3} . See, e.g., Berger (2014) and Kumar & Zhang (2015) for more detailed discussion about the parameters.

In this work we revisit the SSC model for the GRB afterglow emission. We have considered an adiabatic and a radiative blast-wave expansion into a wind-type circumburst medium (wind) and constant density interstellar medium (ISM). These correspond to 4 different scenarios, namely the adiabatic-wind; adiabatic-ISM; radiative-wind and radiative-ISM. Properties of these blast-wave evolution and synchrotron emission from these 4 scenarios have been discussed earlier in Razzaque (2013). Here we reproduce earlier synchrotron results, for completeness, and focus on the SSC component that can potentially explain recently detected VHE emission from GRBs. We apply our model to broadband afterglow data from the bright long GRB 130427A and the bright short GRB 090510, as for illustrations. Our approach in this work is to fix the circumburst medium by the type of the GRB and we consider the wind medium for the long GRB and constant-density medium for the short GRB. We also consider two blast-waves evolving in the circumburst media. The injected energy into the second blast-wave is also taken similar to the gamma-ray observations, which should be consistent with the physical modelling as a fraction of the kinetic energy goes into the gamma rays. For GRB 090510 the isotropic gamma-ray energy is $E_{\gamma, \text{iso}} = 1.1 \times 10^{53} \text{ erg}$ and for the GRB 130427A it is $E_{\gamma, \text{iso}} = 8.1 \times 10^{53} \text{ erg}$ (Panaitescu et al. 2013; Ackermann et al. 2010). The late afterglow has been considered in this work mainly after 100 s, and we have considered the contribution in the late afterglow coming from the forward shock. The reverse shock, which can be important in particular for GRB 130427A, has been discussed by Panaitescu et al. (2013). We model the synchrotron and SSC light curves and the spectral energy distribution (SED) simultaneously for GRBs, to fit the late afterglow emission. We look for the strength of the SSC component and its detectability by the upcoming Cherenkov Telescope Array (CTA) (Cherenkov Telescope Array Consortium et al. 2019).

In Section 2, we discuss the dynamics of the blast-wave, and in Section 3 and 4 the synchrotron and the SSC broadband emission are described, and in Section 5 we describe our modelling of GRB 090510 and GRB 130427A. We summarize our work in Section 6.

2 BLAST-WAVE MODELLING

The GRB event triggers a blast-wave, with injected kinetic energy E_k , into the surrounding medium which slows down with time (Blandford & McKee 1976). Considering the event as a point source, it expands with initial Lorentz factor Γ_0 into the surrounding medium. The GRB blast-wave at radius r would have the

swept-up mass $M_{\text{sw}} = 4\pi m_p n r^3/3$, where n is the gas density of the surrounding medium. The deceleration of the blast-wave would be significant when the energy of the swept-up mass is approximately equal to the injected energy into the blast-wave. The blast-wave moving with Lorentz factor Γ_0 would see the energy of the gas particles blueshifted by $\Gamma_0 m_p c^2$. This energy would be further boosted by Γ_0 in the observer's frame. We consider half of the energy of the ejecta goes into the blast-wave, i.e., $E_k/2 = \Gamma_0^2 M_{\text{sw}} c^2$. The deceleration radius r_d is then

$$r_d = \left(\frac{3E_k}{8\pi\Gamma_0^2 m_p c^2 n} \right)^{1/3}. \quad (1)$$

The deceleration time of the blast-wave measured by the observer is $t_d = (1+z)r_d/2\Gamma_0^2 c$ (Rees & Meszaros 1992), where z is the redshift, can be expressed as

$$t_d = \left[\frac{3E_k(1+z)^3}{64\pi n m_p c^5 \Gamma_0^8} \right]^{1/3}. \quad (2)$$

The deceleration time in the ISM with constant density $n = n_0 \text{ cm}^{-3}$, $E_k = 10^{55} E_{55} \text{ erg}$ and $\Gamma_0 = 10^{2.5} \Gamma_{2.5}$ (with notation $X = 10^n X_n$) can be written as

$$t_{d,i} = \left[\frac{3E_k(1+z)^3}{64\pi n_0 m_p c^5 \Gamma_0^8} \right]^{1/3} = 33.3(1+z)n_0^{-1/3} \Gamma_{2.5}^{-8/3} E_{55}^{1/3} \text{ s}. \quad (3)$$

We also consider a wind medium with density profile $n = AR^{-2}$ and the mass-loss rate by the progenitor star $\dot{M}_w = 10^{-5} \dot{M}_{-5} M_{\odot} \text{ yr}^{-1}$, having a wind velocity $v_w = 10^8 v_8 \text{ cm s}^{-1}$. Therefore $A = \dot{M}/(4\pi v_w m_p) = 3.02 \times 10^{35} A_{\star} \text{ cm}^{-1}$, where $A_{\star} \equiv \dot{M}_{-5}/v_8$. The blast-wave deceleration time in the wind is then

$$t_{d,w} = \left[\frac{E_k(1+z)}{16\pi A m_p c^3 \Gamma_0^4} \right] = 1.5(1+z)A_{\star}^{-1} \Gamma_{2.5}^{-4} E_{55} \text{ s}. \quad (4)$$

The radius $R(t)$ of the blast-wave or the shock front moves with time t after the deceleration time as (Razzaque 2013),

$$R(t) = \frac{2\Gamma^2(t)act}{1+z}, \quad (5)$$

here $a = 4$ and $a = 7$ represent the expansion scenarios for the adiabatic and radiative blast-wave, respectively. Subsequently after the deceleration time, the bulk Lorentz factor for the blast-wave evolve with time in ISM/wind (i/w) as

$$\Gamma_{ad}(t) = \Gamma_0 \left(\frac{t_{d,i/w}}{4t} \right)^{3/8}; \Gamma_{ra}(t) = \Gamma_0 \left(\frac{t_{d,i/w}}{7t} \right)^{3/7}, \quad (6)$$

respectively, in the case of an adiabatic and radiative scenarios. The evolution of the blast-wave radius R and Lorentz factor Γ in the four different scenarios (adiabatic-wind; adiabatic-ISM; radiative-wind and radiative-ISM) are given in the Appendix.

3 SYNCHROTRON EMISSION AND SYNCHROTRON SELF-ABSORPTION

The electrons accelerated at the external shock region radiate away their energy in the amplified magnetic field (see, e.g., Piran 1999; Zhang & Mészáros 2004). The magnetic field takes away a fraction ϵ_B of the total shock energy, and can be expressed as (all jet-frame quantities are denoted with primes)

$$B'(t) = [32\pi\epsilon_B n(R) m_p c^2]^{1/2} \Gamma(t), \quad (7)$$

where $n(R)$ is the ambient medium density, either wind or ISM, and $\Gamma(t)$ is the Lorentz factor of the evolving blast-wave. We report numerical values of the magnetic field in the four different scenarios in the Appendix. We discuss shock-accelerated electron spectrum and characteristic breaks therein next.

3.1 Characteristic electron Lorentz factors

We consider the accelerated electrons follow a power-law spectrum which is defined as $N_e(\gamma'_e) = K\gamma'^{-p}_e$, with spectral index p and normalization $K = (p-1)n'\gamma'^{p-1}_m$. The characteristic Lorentz factor of the accelerated electrons at the forward shock for $p > 2$ is given by (Sari et al. 1998),

$$\gamma'_m(t) = \left[\frac{m_p}{m_e} \epsilon_e \frac{p-2}{p-1} \Gamma(t) \right]; \quad p > 2 \quad (8)$$

The radiation of electrons have two phases of emission called the fast- and slow-cooling. In the fast-cooling, most of the electrons produce the emission efficiently within the dynamic time, while in the slow-cooling, only the high-energy part of the spectrum, above a cooling Lorentz factor γ'_c , cools efficiently. The electron spectrum defined above will be modified in the fast-cooling regime as

$$N_e(\gamma'_e) \propto \begin{cases} \gamma'^{-2}_e; & \gamma'_c \leq \gamma'_e \leq \gamma'_m \\ \gamma'^{-p-1}_e; & \gamma'_e > \gamma'_m, \end{cases} \quad (9)$$

and in the slow-cooling regime as

$$N_e(\gamma'_e) \propto \begin{cases} \gamma'^{-p}_e; & \gamma'_m \leq \gamma'_e \leq \gamma'_c \\ \gamma'^{-p-1}_e; & \gamma'_e > \gamma'_c. \end{cases} \quad (10)$$

The cooling Lorentz factor (γ'_c), can be estimated by comparing the total cooling time $t'_c = 6\pi m_e c / [\sigma_T B'^2 \gamma'_c (1+Y)]$ with the dynamic or expansion time scale $t'_{dyn} = t\Gamma/(1+z)$ as

$$\gamma'_c(t) = \left[\frac{6\pi m_e c^2 (1+z)}{\sigma_T c B'^2(t) t \Gamma(t) (1+Y)} \right]. \quad (11)$$

Here, σ_T is the Thomson cross-section and $Y \equiv L_{IC}/L_{sy}$ is the Comptonization parameter, which is the ratio between the SSC and synchrotron luminosities. In the case of fast-cooling the Y -parameter can be simply expressed as (Sari & Esin 2001)

$$Y(\text{fast}) = \begin{cases} \epsilon_e/\epsilon_B; \epsilon_e/\epsilon_B \ll 1 \\ \sqrt{\epsilon_e/\epsilon_B}; \epsilon_e/\epsilon_B \gg 1 \end{cases} \quad (12)$$

which is valid for all of the 4 different blast-wave evolution scenarios. In the case of slow-cooling the situation is more complicated and we solve relevant equations to obtain

$$Y(\text{slow}) = (\epsilon_e/\epsilon_B)^{1/(4-p)} \times \begin{cases} (t/t_0)^{(2-p)/[2(4-p)]}; & \text{Adiabatic - ISM} \\ (t/t_0)^{(2-p)/(4-p)}; & \text{Adiabatic - Wind} \\ (t/t_0)^{5(2-p)/[7(4-p)]}; & \text{Radiative - ISM} \\ (t/t_0)^{(2-p)/(4-p)}; & \text{Radiative - Wind} \end{cases} \quad (13)$$

We note, however, that a radiative fireball eventually becomes adiabatic when it loses sufficient energy. The transition time t_0 from the fast- to slow-cooling spectra is defined as $\nu_m(t_0) = \nu_c(t_0)$ (Sari et al. 1998).

The saturation Lorentz factor (γ'_s), comes by comparing the accelerating time scale $t'_{acc} = \phi \gamma'_e m_e c / [eB'(t)]$; where ϕ^{-1} is

the acceleration efficiency for electrons; with the total cooling time t'_c defined earlier as,

$$\gamma'_s(t) = \left[\frac{6\pi e}{\phi \sigma_T B'(t) (1+Y)} \right]. \quad (14)$$

Typically $\phi = 10$ is assumed and $\phi = 1$ correspond to the maximum efficiency. Again, we report numerical values and parameter dependence of the characteristic Lorentz factors for different fireball evolution scenarios in the Appendix.

3.2 Synchrotron spectra and break frequencies

The synchrotron break frequencies for the electron Lorentz factors γ'_e are related by the expression (Razzaque 2013),

$$h\nu(t) = \frac{3}{2} \frac{B'(t)}{B_Q} m_e c^2 \frac{\Gamma(t)}{1+z} \gamma'^2_e \quad (15)$$

where $B_Q = 4.41 \times 10^{13}$ G. Using equation (15), we can calculate the synchrotron break frequencies: minimum (ν'_m), cooling (ν'_c) and saturation (ν'_s) from γ'_m , γ'_c and γ'_s , respectively. These frequencies in the jet frame are transformed to the observer frame by the relations $\nu = \nu' \Gamma / (1+z)$. The synchrotron radiation spectrum from these electrons is distributed in particular frequency order, depending on the fast- and slow-cooling (Sari et al. 1998; Granot & Sari 2002; Thomas et al. 2017). The flux of synchrotron radiation is given in the fast-cooling case as

$$F_\nu^f = f_{\nu, \max} \begin{cases} \left(\frac{\nu}{\nu_a}\right)^2 \left(\frac{\nu_a}{\nu_c}\right)^{1/3}; & \nu < \nu_a \\ \left(\frac{\nu}{\nu_c}\right)^{1/3}; & \nu_a \leq \nu \leq \nu_c \\ \left(\frac{\nu}{\nu_c}\right)^{-1/2}; & \nu_c < \nu < \nu_m \\ \left(\frac{\nu}{\nu_m}\right)^{-1/2} \left(\frac{\nu}{\nu_m}\right)^{-p/2}; & \nu \geq \nu_m, \end{cases} \quad (16)$$

and in the slow-cooling as

$$F_\nu^s = f_{\nu, \max} \begin{cases} \left(\frac{\nu}{\nu_a}\right)^2 \left(\frac{\nu_a}{\nu_m}\right)^{1/3}; & \nu < \nu_a \\ \left(\frac{\nu}{\nu_m}\right)^{1/3}; & \nu_a \leq \nu \leq \nu_m \\ \left(\frac{\nu}{\nu_m}\right)^{-(p-1)/2}; & \nu_m < \nu < \nu_c \\ \left(\frac{\nu}{\nu_c}\right)^{-(p-1)/2} \left(\frac{\nu}{\nu_c}\right)^{-p/2}; & \nu \geq \nu_c. \end{cases} \quad (17)$$

Here $f_{\nu, \max}$ is the maximum synchrotron flux density which is defined as (Sari et al. 1998; Razzaque 2013),

$$f_{\nu, \max} = \frac{N}{4\pi d_L^2} \frac{P(\gamma'_m)}{\nu'_m} \frac{\Gamma^2}{(1+z)^2}, \quad (18)$$

with the synchrotron power at γ'_m is given by $P(\gamma'_m) = c\sigma_T B'^2 \gamma'^2_m / 6\pi$ (Rybicki & Lightman 1986). The total number of electrons in the blast-wave is given by $N = (4/3)\pi R^3 n$, and the luminosity distance to the source is given by d_L .

The time-dependence of the synchrotron flux is governed by the time-dependence of $f_{\nu, \max}$ and of various break frequencies. Depending on a particular frequency band being observed, the break frequencies can pass through that band at different times. Two particularly interesting frequencies are ν_m and ν_c , and the time they appear in the spectrum t_m and t_c , respectively, are reported in the Appendix for the four different blast-wave evolution scenarios. The time and frequency evolution of the flux, denoted as $F_\nu \propto t^\alpha \nu^\beta$, give rise to particular relations between α and β for different segments in equations (16) and (17). We report these so-called closure relations (Sari et al. 1998; Granot & Sari 2002; Zhang & Mészáros 2004) for the synchrotron flux in Table 1. The maximum flux $f_{\nu, \max}$ and various break frequencies are reported in the Appendix. We discuss next the synchrotron-self-absorption frequency.

3.3 Synchrotron self-absorption frequency

The synchrotron spectra in equations (16) and (17) have the lowest frequency break at ν_a , below which the synchrotron spectrum becomes harder by index $2/3$ due to synchrotron-self-absorption (Rybicki & Lightman 1986). We describe here the derivation of self-absorption frequency ν_a for the blast-wave in the circumburst medium. To calculate this we first define the self-absorption coefficient based on (Granot et al. 1999),

$$\alpha'_{\nu'} = \frac{p+2}{8\pi m_e \nu'^2} \int_{\gamma_m}^{\infty} P'(\gamma_e) \frac{N_e(\gamma_e)}{\gamma_e} d\gamma_e. \quad (19)$$

Here the electron distribution $N_e(\gamma_e)$ is independent of the fast- and slow-cooling. From the unmodified electron distribution, defined previously we have

$$N_e(\gamma_e) = n'(p-1)\gamma_m^{p-1} \gamma_e^{-p}, \quad (20)$$

where n' is the density of the electrons in the jet frame and is related to the ambient density $n(R)$, with $n' \approx 4\Gamma n(R)$ (Blandford & McKee 1976; Granot et al. 1999) For the electron Lorentz factor γ'_e we can calculate the emitted frequency ν'_{sy} and emitted power $P'(\gamma'_e)$ as (Granot et al. 1999)

$$\nu'_{sy} = \frac{3qB'(t)\gamma_e'^2 \sin \alpha}{4\pi m_e c} \quad (21)$$

and

$$P'(\gamma'_e) = \frac{2^{5/3} \pi e^3 B'(t) \sin \alpha}{\Gamma(\frac{1}{3}) m_e c^2} \left(\frac{\nu'}{\nu'_{sy}} \right)^{1/3}, \quad (22)$$

respectively. Here, Γ represents the Gamma function. Using equations (19-22) we can derive the expression for the self-absorption coefficient as

$$\alpha'_{\nu'} = \frac{(p+2)(p-1)n'}{8\pi m_e \nu'^{5/3}} \frac{2^{5/3} \pi q_e^3 B'(t) \sin \alpha}{\Gamma(\frac{1}{3}) m_e c^2} \times \left[\frac{4\pi m_e c}{3q_e B'(t) \sin \alpha} \right]^{1/3} \gamma_m^{p-1} \int_{\gamma'_m}^{\infty} \gamma_e^{-(p+5/3)} d\gamma_e. \quad (23)$$

We further simplified this expression using an average value of $\sin^{3/2} \alpha$, which is equal to $(\sqrt{\pi}/5)\Gamma(1/3)\Gamma(5/6)$, as

$$\alpha'_{\nu'} = 4.72 \times 10^{-10} \left[\frac{(p+2)(p-1)}{(3p+2)\nu'^{5/3}} \right] q_e^{8/3} m_e^{-5/3} \times m_p^{1/3} \epsilon_B^{1/3} \Gamma(t)^{5/3} n(R)^{4/3} \gamma_m^{-5/3}. \quad (24)$$

In the expansion into ISM, $n(R) = n_0$ is a constant density and for wind case it follows the relation $n(R) \propto 1/R^2$ distribution. We derive the absorption coefficients in these two cases as

$$\alpha'_{\nu'}(\text{ISM}) = 925.6 \frac{(p+2)(p-1)}{(3p+2)\nu'^{5/3}} \epsilon_B^{1/3} n_0^{4/3} \gamma_m^{-5/3} \Gamma(t)^{5/3} \quad (25)$$

and

$$\alpha'_{\nu'}(\text{Wind}) = 1.88 \times 10^{50} \frac{(p+2)(p-1)}{(3p+2)\nu'^{5/3}} \times \epsilon_B^{1/3} A_*^{4/3} R(t)^{-8/3} \gamma_m^{-5/3} \Gamma(t)^{5/3}, \quad (26)$$

respectively.

From the above expressions of $\alpha'_{\nu'}$, at the absorption frequency $\nu' = \nu'_a$, the condition that must be satisfied is $\alpha'_{\nu'} R(t)/\Gamma(t) = 1$. Further, following Dermer & Menon (2009) for the slow-cooling case $\gamma'_e = \gamma'_m$ and for the fast-cooling case

$\gamma'_e = \gamma'_c$ provides the general expression for the synchrotron-self-absorption frequency as

$$\nu'_{a[s,f]}(\text{ISM}) = 1851.2 \frac{(p+2)(p-1)}{(3p+2)} \times \left[\epsilon_B^{1/3} n_0^{4/3} \gamma_{[m,c]}^{-5/3} \Gamma(t)^{8/3} \frac{act}{1+z} \right]^{3/5} \quad (27)$$

and

$$\nu'_{a[s,f]}(\text{Wind}) = 5.83 \times 10^{49} \frac{(p+2)(p-1)}{(3p+2)} \times \left[\epsilon_B^{1/3} A_*^{4/3} \gamma_{[m,c]}^{-5/3} \Gamma(t)^{-8/3} \left(\frac{act}{1+z} \right)^{-5/3} \right]^{3/5}, \quad (28)$$

respectively, for the ISM and wind medium. The subscripts $[s, f] \rightarrow [m, c]$ refer to the slow- and fast-cooling cases. The self-absorption frequency depends on the spectral index p of the electrons for both the fast- and slow-cooling scenarios, due to their dependence on the minimum Lorentz factor γ'_m . We report numerical values of ν_a in the Appendix for different blast-wave evolution scenarios.

4 SYNCHROTRON SELF-COMPTON EMISSION

The inverse-Compton spectrum for the same electrons up-scattering synchrotron photons in the Thomson regime is approximated by a power-law segment with break frequencies given, following Sari & Esin (2001), by

$$\begin{aligned} \nu_a^{\text{IC}} &= 2\gamma_m'^2 \nu_a \\ \nu_m^{\text{IC}} &= 2\gamma_m'^2 \nu_m \\ \nu_c^{\text{IC}} &= 2\gamma_c'^2 \nu_c \end{aligned} \quad (29)$$

For this component of the spectrum we follow a similar flux distribution as for the synchrotron part with a shift in frequency as defined above. Similar to the maximum synchrotron flux $f_{\nu, \text{max}}$ in equation (18), we define the maximum SSC flux, which is based on the formalism discussed in Zhang & Mészáros (2001), as

$$f_{\nu, \text{max}}^{\text{IC}} = \frac{\nu_m^{sy} U'_{\text{ph}}}{\nu_m^{\text{IC}} U'_B} f_{\nu, \text{max}}. \quad (30)$$

Here the magnetic energy density is $U'_B = B'^2/8\pi$ and the photon energy density is $U'_{\text{ph}} = (16/3)\sigma_T U'_B \gamma_m'^2 R(t)n(R)$. The SSC component produced in our approximation slightly deviates at higher energies compared to the integrated spectrum of electrons scattered by the seed photons, as discussed in Sari & Esin (2001) and its effects are small.

The fast- and slow-cooling SSC spectra in the Thomson regime follow the same ordering as for the synchrotron spectra. From the flux distribution we can calculate its dependence on the frequency and time, $F_\nu \propto \nu^\alpha t^\beta$, for all possible SSC scenarios of blast-wave expansion are given in our Table 2. The Klein-Nishina effect, however, can become important for SSC emission at very-high energies, which we discuss next.

4.1 Klein-Nishina cutoff energies

The Klein-Nishina effect in the IC scattering is important for electrons with Lorentz factor above $\gamma'_{\text{KN}} = mc^2/h\nu'$, for scattering photons of frequency ν' in the jet frame. This corresponds to a

maximum IC photon frequency $2\gamma_{\text{KN}}^2\nu'$. From equation (29), we obtain two relevant Klein-Nishina limiting frequencies as

$$\nu_{m/c, \text{KN}}^{\text{IC}} = \frac{2m^2c^4}{h^2\nu_{m/c}} \frac{\Gamma^2}{(1+z)^2} \quad (31)$$

Photons above this energy are produced inefficiently and their flux decreases. We take the higher value between $\nu_{m, \text{KN}}^{\text{IC}}$ and $\nu_{c, \text{KN}}^{\text{IC}}$ as the maximum frequency. We report all IC frequencies, including this Klein-Nishina limiting frequencies, for different blast-wave evolution scenarios in the Appendix.

5 MODELLING OF BROAD-BAND AFTERGLOW EMISSION

We apply our modelling to two bright GRBs, namely the short GRB 090510 and the long GRB 130427A, which have been observed in radio to gamma-rays. We fit simultaneously the broad-band spectral energy distributions (SEDs) at different time after the burst and light curves at different frequencies. We found that a single blast-wave is not adequate to explain data for either GRB. Reasonable fits are obtained with two blast-waves (jet inside jet) as discussed previously for other GRB afterglows (see, e.g., Zheng & Deng 2010; Corsi et al. 2010; Filgas et al. 2011; Holland et al. 2012). We have also added the SSC component in our modelling which is relevant for the recent MAGIC and HESS observations of VHE emission from GRBs.

5.1 Short GRB 090510

The GRB 090510 with a duration of $T_{90} = 0.3 \pm 0.07$ s was observed in the early afterglow phase by the Swift and Fermi satellites (De Pasquale et al. 2010). The redshift of the burst is $z = 0.903 \pm 0.003$ (Rau et al. 2009). These observations were modeled using typical synchrotron radiation (De Pasquale et al. 2010); an electron-proton synchrotron model (Razzaque 2010), where the proton component was used to interpret the Fermi-LAT data; and a two-component jet model (Corsi et al. 2010).

In this work, we fit the SED and light curves of GRB 090510 with two adiabatic blast-waves in a very low and constant density environment. We take into account total cooling effects on the electrons, synchrotron and Compton, in the forward shock, and constrain the afterglow model parameters from the multiwavelength observations. The deceleration times of around 28 and 30 s for both the blast-waves and the cooling time for electrons is such that the afterglow which are shown from 100 s are explained using the slow-cooling of the electrons. One blast-wave dominantly contribute to the observed multiwavelength data. Slight contribution is added from a second blast-wave which is ejected at the same time but with slightly lower energy and lower initial Lorentz factor.

Figure 1 shows the data and our model curves for GRB 090510. The optical and X-ray data interpretation favours a very low circumburst density of 10^{-5} cm^{-3} . The fast decay of the flux at late times is also connected to the jet-break, which appears at $\Gamma \sim \theta_0^{-1}$ (Sari et al. 1999), where θ_0 is the jet opening angle and $t_{\text{jet}} = 5 \times 10^5 (1+z)(E_{55}/n)^{1/3} \theta_{-1}^{8/3}$ s is the jet-brak time. We find the jet-break time is in the range of 1.4-5.1 ks, as discussed in Razzaque (2010). After the jet-break, the time dependence is $\nu_a \propto t^{-1/5}$, $\nu_m \propto t^{-2}$, and $\nu_c \propto t^0$ and the maximum flux $f_{\nu, \text{max}} \propto t^{-1}$. These dependencies also modify the SSC signal for the adiabatic blast-wave into the constant density medium. The

Table 1. The closure relations between the temporal index α and spectral index β in various afterglow models for synchrotron emission.

	β	α	$\alpha(\beta)$
Adiabatic (ISM) slow cooling			
$\nu < \nu_{a,s}$	2	$\frac{1}{2}$	$\frac{\beta}{1}$
$\nu_{a,s} \leq \nu \leq \nu_{m,s}$	$\frac{1}{3}$	$\frac{1}{2}$	$\frac{3\beta}{2}$
$\nu_{m,s} < \nu < \nu_{c,s}$	$\frac{-(p-1)}{2}$	$-\frac{3(p-1)}{2}$	$\frac{3\beta}{2}$
$\nu \geq \nu_{c,s}$	$\frac{-p}{2}$	$-\frac{(3p-2)}{4}$	$\frac{(3\beta+1)}{2}$
Adiabatic (ISM) fast cooling			
$\nu < \nu_{a,s}$	2	1	$\frac{\beta}{2}$
$\nu_{a,s} \leq \nu \leq \nu_{c,s}$	$\frac{1}{3}$	$\frac{1}{6}$	$\frac{\beta}{2}$
$\nu_{c,s} < \nu < \nu_{m,s}$	$\frac{-1}{2}$	$\frac{-1}{4}$	$\frac{\beta}{2}$
$\nu \geq \nu_{m,s}$	$\frac{-p}{2}$	$-\frac{(3p-2)}{4}$	$\frac{(3\beta+1)}{2}$
Adiabatic (wind) slow cooling			
$\nu < \nu_{a,s}$	2	1	$\frac{\beta}{2}$
$\nu_{a,s} \leq \nu \leq \nu_{m,s}$	$\frac{1}{3}$	0	$\frac{(3\beta-1)}{2}$
$\nu_{m,s} < \nu < \nu_{c,s}$	$\frac{-(p-1)}{2}$	$-\frac{(3p-1)}{4}$	$\frac{(3\beta-1)}{2}$
$\nu \geq \nu_{c,s}$	$\frac{-p}{2}$	$-\frac{3p-2}{4}$	$\frac{(3\beta+1)}{2}$
Adiabatic (wind) fast cooling			
$\nu < \nu_{a,s}$	2	2	β
$\nu_{a,s} \leq \nu \leq \nu_{c,s}$	$\frac{1}{3}$	$\frac{-2}{3}$	$\frac{-(\beta+1)}{2}$
$\nu_{c,s} < \nu < \nu_{m,s}$	$\frac{-1}{2}$	$\frac{-1}{4}$	$\frac{-(\beta+1)}{2}$
$\nu \geq \nu_{m,s}$	$\frac{-p}{2}$	$-\frac{(3p-2)}{4}$	$\frac{(3\beta+1)}{2}$
Radiative (ISM) slow cooling			
$\nu < \nu_{a,s}$	2	$\frac{5}{7}$	$\frac{5\beta}{14}$
$\nu_{a,s} \leq \nu \leq \nu_{m,s}$	$\frac{1}{3}$	$\frac{4}{7}$	$\frac{12\beta}{7}$
$\nu_{m,s} < \nu < \nu_{c,s}$	$\frac{-(p-1)}{2}$	$-\frac{6(p-1)}{7}$	$\frac{12\beta}{7}$
$\nu \geq \nu_{c,s}$	$\frac{-p}{2}$	$-\frac{(6p-5)}{7}$	$\frac{(12\beta+5)}{7}$
Radiative (ISM) fast cooling			
$\nu < \nu_{a,s}$	2	$\frac{10}{7}$	$\frac{5\beta}{7}$
$\nu_{a,s} \leq \nu \leq \nu_{c,s}$	$\frac{1}{3}$	$\frac{2}{21}$	$\frac{2\beta}{7}$
$\nu_{c,s} < \nu < \nu_{m,s}$	$\frac{-1}{2}$	$\frac{-1}{7}$	$\frac{2\beta}{7}$
$\nu \geq \nu_{m,s}$	$\frac{-p}{2}$	$-\frac{(6p-5)}{7}$	$\frac{(12\beta+5)}{7}$
Radiative (wind) slow cooling			
$\nu < \nu_{a,s}$	2	$\frac{4}{3}$	$\frac{2\beta}{3}$
$\nu_{a,s} \leq \nu \leq \nu_{m,s}$	$\frac{1}{3}$	$\frac{5}{9}$	$\frac{5\beta}{3}$
$\nu_{m,s} < \nu < \nu_{c,s}$	$\frac{-(p-1)}{2}$	$-\frac{5(p-1)}{6}$	$\frac{5\beta}{3}$
$\nu \geq \nu_{c,s}$	$\frac{-p}{2}$	$-\frac{(5p-6)}{6}$	$\frac{(5\beta+3)}{3}$
Radiative (wind) fast cooling			
$\nu < \nu_{a,s}$	2	$\frac{7}{3}$	$\frac{7\beta}{6}$
$\nu_{a,s} \leq \nu \leq \nu_{c,s}$	$\frac{1}{3}$	$\frac{-1}{9}$	$\frac{-\beta}{3}$
$\nu_{c,s} < \nu < \nu_{m,s}$	$\frac{-1}{2}$	$\frac{1}{6}$	$\frac{-\beta}{3}$
$\nu \geq \nu_{m,s}$	$\frac{-p}{2}$	$-\frac{(5p-6)}{6}$	$\frac{(5\beta+3)}{3}$

breaks in the relevant time range for GRB 090510, of the first component are: Optical ($t_m = 776.32$ s), LAT ($t_m^{\text{SSC}} = 75.8$ s). For the second component, Optical ($t_m = 7025.17$ s) XRT ($t_m = 103.95$ s), LAT ($t_m^{\text{SSC}} = 599.4$ s). All the light curves are shown with jet-break after 5 ks.

Figure 1 (top panel) also shows the differential flux sensitivity of CTA to transient sources. In such calculations, a 5σ significance is required in each energy bin and the source flux needs to

Table 2. The closure relations between the temporal index α and spectral index β in various afterglow models for SSC emission.

	β	α	$\alpha(\beta)$
Adiabatic(ISM) slow cooling			
$\nu < \nu_{a,ic}$	2	2	β
$\nu_{a,ic} \leq \nu \leq \nu_{m,ic}$	$\frac{1}{3}$	$\frac{3}{4}$	$\frac{9\beta}{4}$
$\nu_{m,ic} < \nu < \nu_{c,ic}$	$\frac{-(p-1)}{2}$	$\frac{-9(p-1)}{8}$	$\frac{9\beta}{4}$
$\nu \geq \nu_{c,ic}$	$\frac{-p}{2}$	$\frac{-(9p-8)}{8}$	$\frac{(9\beta+4)}{4}$
Adiabatic(ISM) fast cooling			
$\nu < \nu_{a,ic}$	2	2	β
$\nu_{a,ic} \leq \nu \leq \nu_{c,ic}$	$\frac{1}{3}$	$\frac{1}{12}$	$\frac{\beta}{4}$
$\nu_{c,ic} < \nu < \nu_{m,ic}$	$\frac{-1}{2}$	$\frac{-1}{8}$	$\frac{\beta}{4}$
$\nu \geq \nu_{m,ic}$	$\frac{-p}{2}$	$\frac{-(9p-8)}{8}$	$\frac{(9\beta+4)}{4}$
Adiabatic (wind) slow cooling			
$\nu < \nu_{a,ic}$	2	$\frac{5}{2}$	$\frac{5}{4}\beta$
$\nu_{a,ic} \leq \nu \leq \nu_{m,ic}$	$\frac{1}{3}$	$\frac{2}{3}$	2β
$\nu_{m,ic} < \nu < \nu_{c,ic}$	$\frac{-(p-1)}{2}$	$-(p-1)$	2β
$\nu \geq \nu_{c,ic}$	$\frac{-p}{2}$	$-(p-2)$	$(2\beta+2)$
Adiabatic (wind) fast cooling			
$\nu < \nu_{a,ic}$	2	0	$\beta-2$
$\nu_{a,ic} \leq \nu \leq \nu_{c,ic}$	$\frac{1}{3}$	$\frac{-1}{6}$	$\frac{-\beta}{2}$
$\nu_{c,ic} < \nu < \nu_{m,ic}$	$\frac{-1}{2}$	1	$\frac{-\beta}{2}$
$\nu \geq \nu_{m,ic}$	$\frac{-p}{2}$	$-(p-2)$	$(2\beta+2)$
Radiative (ISM) slow cooling			
$\nu < \nu_{a,ic}$	2	$\frac{17}{7}$	$\frac{17\beta}{7}$
$\nu_{a,ic} \leq \nu \leq \nu_{m,ic}$	$\frac{1}{3}$	$\frac{6}{7}$	$\frac{18\beta}{7}$
$\nu_{m,ic} < \nu < \nu_{c,ic}$	$\frac{-(p-1)}{2}$	$\frac{-9(p-1)}{7}$	$\frac{18\beta}{7}$
$\nu \geq \nu_{c,ic}$	$\frac{-p}{2}$	$\frac{(-9p+10)}{7}$	$\frac{(18\beta+10)}{7}$
Radiative (ISM) fast cooling			
$\nu < \nu_{a,ic}$	2	$\frac{10}{7}$	$\frac{5\beta}{7}$
$\nu_{a,ic} \leq \nu \leq \nu_{c,ic}$	$\frac{1}{3}$	$\frac{2}{7}$	$\frac{7\beta}{7}$
$\nu_{c,ic} < \nu < \nu_{m,ic}$	$\frac{-1}{2}$	$\frac{-1}{7}$	$\frac{7\beta}{7}$
$\nu \geq \nu_{m,ic}$	$\frac{-p}{2}$	$\frac{-(6p-5)}{7}$	$\frac{(12\beta+5)}{7}$
Radiative (wind) slow cooling			
$\nu < \nu_{a,ic}$	2	$\frac{8}{3}$	$\frac{4\beta}{3}$
$\nu_{a,ic} \leq \nu \leq \nu_{m,ic}$	$\frac{1}{3}$	$\frac{7}{9}$	$\frac{7\beta}{3}$
$\nu_{m,ic} < \nu < \nu_{c,ic}$	$\frac{-(p-1)}{2}$	$\frac{7(p-1)}{9}$	$\frac{7\beta}{3}$
$\nu \geq \nu_{c,ic}$	$\frac{-p}{2}$	$\frac{-(7p-12)}{6}$	$\frac{(7\beta+6)}{3}$
Radiative (wind) fast cooling			
$\nu < \nu_{a,ic}$	2	$\frac{-1}{3}$	$\frac{-\beta}{6}$
$\nu_{a,ic} \leq \nu \leq \nu_{c,ic}$	$\frac{1}{3}$	$\frac{-5}{9}$	$\frac{-5\beta}{3}$
$\nu_{c,ic} < \nu < \nu_{m,ic}$	$\frac{-1}{2}$	$\frac{5}{6}$	$\frac{-5\beta}{3}$
$\nu \geq \nu_{m,ic}$	$\frac{-p}{2}$	$\frac{-(7p-12)}{6}$	$\frac{(7\beta+6)}{3}$

be few times higher than the background signal. These sensitivities for 25 events in each bin, where 4 bins are taken per decade of energy, is calculated by Funk et al. (2013). These calculation shows differential flux sensitivity of CTA for 25 GeV gamma-rays is approximately 10^{-9} erg cm $^{-2}$ s $^{-1}$ if the transient source lifetime is considered to be within 10 s. In our work we have used the CTA

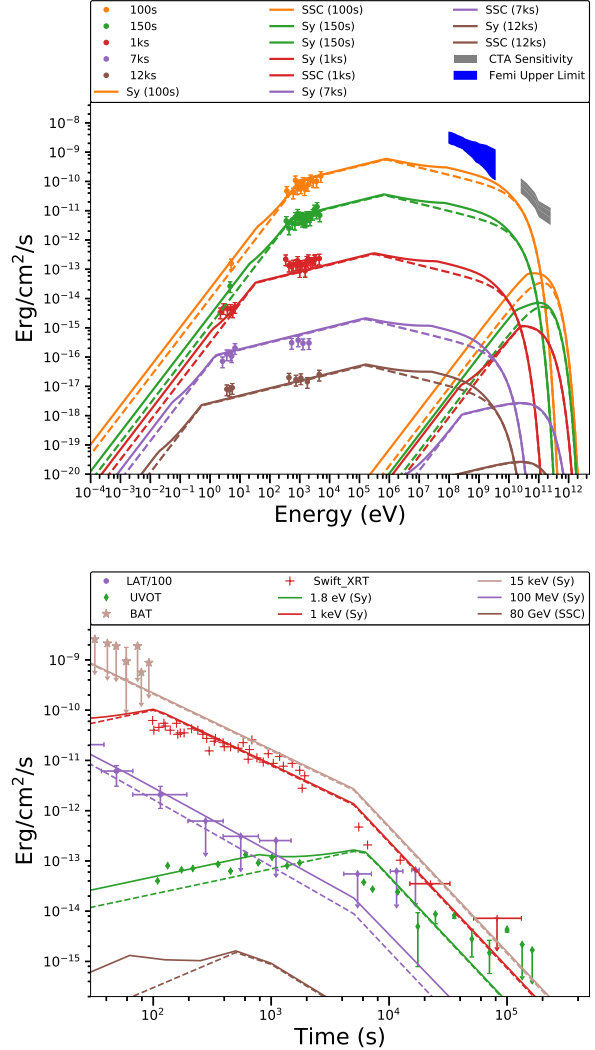


Figure 1. *Top Panel:* The SED of short GRB 090510, where the multiwavelength data are shown for the Swift and Fermi-LAT observations (De Pasquale et al. 2010). *Bottom Panel:* The Swift/BAT (15-350 keV), Swift/UVOT, and Swift/XRT (0.3-10keV), Fermi-LAT (100 MeV-4 GeV) light curves are shown. For the duration 1.9-5.1 ks, there are no data points in Swift/XRT observation due to Earth occultation. The data points are taken from De Pasquale et al. (2010) and the SED fluxes are scaled by factors 1, 10, 10 2 , 10 3 and 10 4 in decreasing order of time. The solid lines in both curves show the total emission and the dashed lines with the same color shows the importance of the second component.

sensitivity for transients calculated at an elevation angle 70 $^\circ$, which has been retrieved from the CTA website¹.

5.2 Long GRB 130427A

One of the brightest long GRB 130427A with $T_{90} = 276 \pm 5$ s was located at redshift $z = 0.34$ (Levan et al. 2013). The afterglow of GRB 130427A was observed up to 220 ks in radio and optical wavelengths while the X-ray and gamma-ray observations by Swift-XRT and Fermi-LAT were active upto 1.8 ks (Maselli et al.

¹ <https://www.cta-observatory.org/science/cta-performance/>

Table 3. The afterglow model parameters from our fitting. In GRB 130427A the progenitor star wind medium has $A_* = 0.007$ and the GRB 090510 has a circumburst medium of constant density $n_0 = 10^{-5} \text{cm}^{-3}$.

Parameter	GRB 090510		GRB 130427A	
	Inner jet	Outer jet	Inner jet	Outer jet
E_k (erg)	4×10^{53}	10^{53}	5.3×10^{54}	10^{54}
Γ_0	1200	1000	1000	500
t_{dec} (s)	28.0	29.5	1.5	4.6
t_0 (s)	0.0006	0.36	51.8	31.42
t_{jbrk} (s)	5000	5000	-	-
p	2.4	2.5	2.13	2.01
ϵ_e	0.1	0.2	0.35	0.3
ϵ_B	0.001	0.1	0.011	0.3
ϕ	1.0	1.0	1.0	1.0

2014). A photon of energy 95 GeV was detected at $T_0 + 244$ s and a 32 GeV photon was detected in late time at $T_0 + 34.4$ ks (Ackermann et al. 2014). Its association with a type-Ic supernova (Melandri et al. 2014a) provides us further evidence that long GRB 130427A is produced by the collapse of a massive star. The afterglow data from GRB 130427A have been modelled when the shock interacts with the external medium and synchrotron and SSC mechanism can explain the afterglow emission (Panaitescu et al. 2013; Laskar et al. 2013; Liu et al. 2013).

We model the afterglow emission after T_{90} , and the model parameters are constrained by the simultaneous interpretation of the SED and light curves. We consider that two blast-waves were ejected from the central engine with initial Lorentz factors $\Gamma_{0,1}$ and $\Gamma_{0,2}$, where $\Gamma_{0,1} > \Gamma_{0,2}$. Note that the radio emission observed at later time after 10^5 s is not explained using a single blast-wave model (Maselli et al. 2014). The circumburst environment of GRB 130427A in this work has been assumed to be a wind medium. This assumption is supported by the fact that it is a long GRB and it was associated with a type-Ic supernovae (Melandri et al. 2014b).

The inner jet is launched with a larger Lorentz factor and the outer jet with a smaller Lorentz factor. The outer jet has full contribution to radio and some fraction in the optical wavelengths, as shown in Figure 2. The inner jet produces fraction of emission in optical and a full contribution to the X-rays and gamma rays. The breaks in the relevant time range for GRB 130427A, of the first component are: Radio ($t_a = 646.09$ s), Optical ($t_m = 3741.35$ s). For the second component, Radio ($t_a = 1293$, $t_m = 343020.35$ s), Optical ($t_m = 199.8$ s).

5.3 Maximum photon energy

The maximum photon energy is constrained by different factors: a) maximum synchrotron energy; b) Klein-Nishina (KN) effect for SSC; c) $\gamma\gamma \rightarrow e^\pm$ pair creation; and d) absorption in the extragalactic background light (EBL). A combination of all these factors can also be at play. We discuss these in more details below

The maximum photon energy by the synchrotron mechanism is given by $h\nu_s$. The synchrotron cut-off energy $h\nu_s$ for the times 100 s-12 ks in Fig. 1 top panel are 5.05, 4.33, 2.12, 1.02, 0.84 GeV for the inner jet of GRB 090510. For the outer jet the cut-off energies are 19.35, 16.62, 8.15, 3.93, 3.21 GeV. In Fig. 2 top panel the cut-off energy for GRB 130427A for the times 352 s-220 ks has values 5.45, 5.3, 4.74, 3.6, 2.42, 2.01, 1.55 GeV for the inner jet. For the outer jet the cut-off energies are

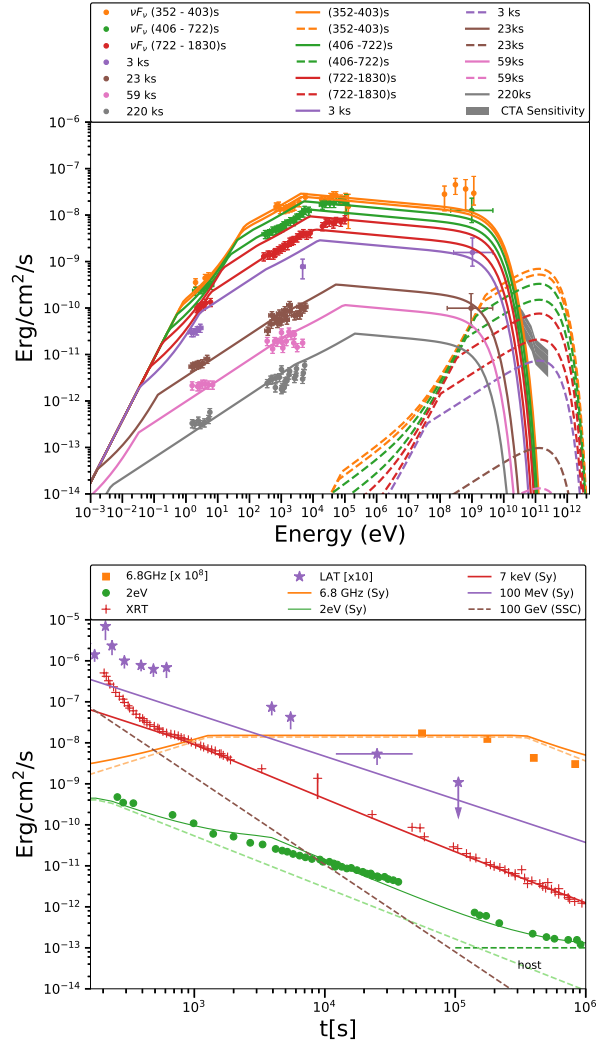


Figure 2. *Top Panel:* The SED of the long GRB 130427A, where the total contribution from two component is shown. The contribution of the second component is shown in a separate figure in the Appendix to illustrate the contrast in contributions. *Bottom Panel:* . The solid lines in the light curve are for the total contribution from the two components, while the dashed lines in the same color show the contribution from the second component. The parameters used for the two components are shown in Table 3. The data used in these two plots XRT (0.3-10) keV, Radio (6.8 GHz), LAT (0.1-100 GeV) are taken from (Maselli et al. 2014).

10.64, 10.27, 8.9, 6.26, 3.78, 3, 2.16 GeV. The maximum synchrotron photon energy is not a limiting factor for the cases when the Compton parameter $Y > 1$. The maximum SSC photon energy in the Thomson limit is $h\nu_s^{\text{IC}}$ and in principle it can be very high. However, the KN effect reduces the maximum energy of the SSC photons to lower energies. Here, for simplicity, we calculate the KN limiting energies for the inner jet parameters, as similar values are expected for the outer jet.

In the case of GRB 090510 and GRB 130427A afterglows, the KN energies are 741 TeV and 13.7 TeV at the earliest times of the SED plotted in Figs. 1 and 2, respectively. These values for the later times can be calculated based on the expressions for $h\nu_c^{\text{IC,KN}}$ and $h\nu_m^{\text{IC,KN}}$. As defined in Section 4.1, the maximum of these values is taken as the KN energy value.

The $\gamma\gamma \rightarrow e^\pm$ pair production optical depth for gamma rays,

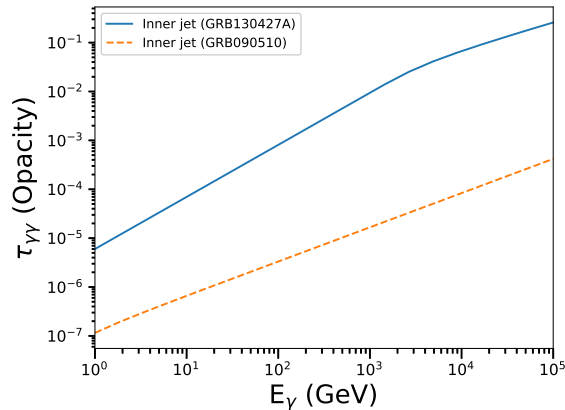


Figure 3. The optical depths versus the observed photon energy in the target photon field are shown for the inner jet parameters at 100 s for GRB090510 and at 352 s for GRB130427A, respectively. At these times, the radius of the blast-waves for these two GRBs have values 2.5×10^{18} cm and 2.1×10^{18} cm. The optical depth in the jet is rather small for both the GRBs for up to the KN energies and the EBL absorption energies.

in the target synchrotron radiation field of the jet, is calculated for both the GRBs following Gould & Schröder (1967). We calculate the optical depth for gamma rays at the peak flux in the synchrotron target radiation field. In Fig. 3 we have shown the gamma-gamma opacity for VHE photons and it is not very effective to attenuate the VHE gamma rays produced by SSC during the afterglows in GRB 090510 and GRB 130427A for up to at least 100 TeV. These VHE photons will escape from the GRBs but due to large redshifts of the GRBs considered in this work, the EBL attenuation is important. We use the EBL model by Finke et al. (2010), which allows ~ 300 GeV photon-energy limit for GRB 130427A and ~ 100 GeV for GRB 090510, when the optical depth is of the order 1. In Figs. 1 and 2 we have shown the EBL cutoffs in the SSC spectra. In principle, gamma rays absorbed in the EBL can initiate a cascade and secondary contributions to the overall emission can be important if the intergalactic magnetic field is $\lesssim 10^{-19}$ G (see, e.g., Razzaque et al. 2004; Ando 2004; Murase et al. 2007).

6 SUMMARY AND DISCUSSION

We have calculated the synchrotron and SSC afterglow emission from GRBs in this work using the external forward shock model. We have derived detailed formulas to compute these emission components in four different blast-wave evolution scenarios in order to fit temporal evolution of the broadband SEDs and radio to VHE gamma-ray light curves. We have also derived the so-called closure relations between temporal and spectral dependence of the synchrotron and SSC fluxes, that are useful for fitting multiwavelength afterglow data from GRBs and extract model parameters. A numerical code has been developed to use our formalism for such fittings to current and future data from GRBs. We have applied this code to fit multiwavelength data from two bright GRBs, namely GRB 090510 and GRB 130427A.

We found synchrotron dominance in GRB 090510 compared to the SSC signal and the jet-break features are observed at 5 ks. For GRB 130427A the SSC signal shows peak fluxes which are above the CTA sensitivity limits for up to 1 ks, if similar kind of burst occurs during its operation. The expansion of the GRB blast-wave

is considered to be adiabatic for the modelling of GRB 130427A and GRB 090510 at late times as we have considered. The two-component jet model used in this work has some advantage, in particular for GRB 090510, for which we can explain the early-time high brightness in gamma rays and lower contribution in early optical emission. In GRB 130427A its emission is important in tuning the optical-UV emission at early times, till the duration 722-1830 s and it also produces a flat radio component at 6.8 GHz. The 6.8 GHz radio component based on our model should be observed for all times during afterglow, which has been observed after 70 ks.

For our two-component model for GRB 090510 we required 10^{-5} cm $^{-3}$ ISM density which is 10 times higher than the two component model by Corsi et al. (2010), who didn't fit the SEDs unlike here. This difference might be due to other input parameters. We show that if the second component triggers at the same time with the first component, their combination can explain the afterglow emission after the deceleration time ~ 30 s. Assuming if more than one component is also true for GRB 130427A, we check the possible parameter space for explaining the multiwavelength observations till 10^5 of GeV energy by the synchrotron component. The SSC emission shows a distinct component, which is significant in comparison to the CTA sensitivity for transients. The progenitor star wind environment with a wind loss-rate of $7 \times 10^{-8} M_{\odot} \text{yr}^{-1}$ found to be very similar to the afterglow model by Panaitescu et al. (2013). The two component afterglow model can therefore interpret the observed afterglow data very well. In case of GRB 130427A, the Fermi-LAT gamma-ray light curve during the early 352-403 s can-not be well explained. Additional contribution in the late time optical emission by the host galaxy may also be needed.

In conclusions, our synchrotron-SSC modelling proves to be useful in fitting multiwavelength afterglow data from GRBs. Applications to future GRBs, including VHE data, will be extremely interesting to shed lights on the GRB blast-wave models and physical parameters involved in radio to VHE gamma-ray emission.

7 ACKNOWLEDGEMENTS

The research work of J.C.J. was supported by a GES fellowship at the University of Johannesburg, where most part of the work is completed. We are thankful to X.-Y. Wang for reading the manuscript and his comments and to R. J. Britto for providing the python script for the optical depth calculation. S.R. acknowledges support from the National Research Foundation (South Africa) with Grant No. 111749 (CPRR).

REFERENCES

- Ackermann M. et al., 2014, *Science*, 343, 42
- Ackermann M. et al., 2010, *ApJ*, 716, 1178
- Ajello M. et al., 2019, arXiv e-prints, arXiv:1909.10605
- Ando S., 2004, *MNRAS*, 354, 414
- Berger E., 2014, *ARA&A*, 52, 43
- Blandford R. D., McKee C. F., 1976, *Physics of Fluids*, 19, 1130
- Cherenkov Telescope Array Consortium et al., 2019, *Science with the Cherenkov Telescope Array*
- Chevalier R. A., Li Z.-Y., 2000, *ApJ*, 536, 195
- Chiang J., Dermer C. D., 1999, *ApJ*, 512, 699
- Corsi A., Guetta D., Piro L., 2010, *ApJ*, 720, 1008
- Costa E. et al., 1997, *Nature*, 387, 783
- de Naurois M., 2019, *The Astronomer's Telegram*, 13052, 1
- De Pasquale M. et al., 2010, *ApJ*, 709, L146
- Derishev E., Piran T., 2019, *ApJ*, 880, L27

- Dermer C. D., Menon G., 2009, High Energy Radiation from Black Holes: Gamma Rays, Cosmic Rays, and Neutrinos, Princeton University Press
- Filgas R. et al., 2011, *A&A*, 526, A113
- Finke J. D., Razzaque S., Dermer C. D., 2010, *ApJ*, 712, 238
- Fraija N., Barniol Duran R., Dichiarà S., Beniamini P., 2019a, *ApJ*, 883, 162
- Fraija N., Dichiarà S., Pedreira A. C. C. d. E. S., Galvan-Gamez A., Baccera R. L., Barniol Duran R., Zhang B. B., 2019b, *ApJ*, 879, L26
- Fraija N. et al., 2019c, arXiv e-prints, arXiv:1905.13572
- Funk S., Hinton J. A., CTA Consortium, 2013, *Astroparticle Physics*, 43, 348
- Gehrels N., Razzaque S., 2013, *Frontiers of Physics*, 8, 661
- Ghisellini G., Ghirlanda G., Nava L., Celotti A., 2010, *MNRAS*, 403, 926
- Gould R. J., Schröder G. P., 1967, *Phys. Rev.*, 155, 1404
- Granot J., Piran T., Sari R., 1999, *ApJ*, 527, 236
- Granot J., Sari R., 2002, *ApJ*, 568, 820
- Holland S. T. et al., 2012, *ApJ*, 745, 41
- Kumar P., Barniol Duran R., 2009, *MNRAS*, 400, L75
- Kumar P., Zhang B., 2015, *Phys. Rep.*, 561, 1
- Laskar T. et al., 2013, *ApJ*, 776, 119
- Levan A. J., Cenko S. B., Perley D. A., Tanvir N. R., 2013, *GRB Coordinates Network*, 14455, 1
- Liu R.-Y., Wang X.-Y., Wu X.-F., 2013, *ApJ*, 773, L20
- Maselli A. et al., 2014, *Science*, 343, 48
- Melandri A. et al., 2014b, *A&A*, 567, A29
- Melandri A. et al., 2014a, *A&A*, 567, A29
- Meszáros P., Rees M. J., 1994, *MNRAS*, 269, L41
- Mészáros P., Rees M. J., 1997, *ApJ*, 476, 232
- Mirzoyan R. et al., 2019, *GRB Coordinates Network*, 23701, 1
- Murase K., Asano K., Nagataki S., 2007, *ApJ*, 671, 1886
- Paczynski B., Rhoads J. E., 1993, *ApJ*, 418, L5
- Panaitescu A., Kumar P., 2001, *ApJ*, 560, L49
- Panaitescu A., Mészáros P., 1999, *ApJ*, 526, 707
- Panaitescu A., Vestrand W. T., Woźniak P., 2013, *MNRAS*, 436, 3106
- Piel Q. et al., 2019, in *International Cosmic Ray Conference*, Vol. 36, 36th International Cosmic Ray Conference (ICRC2019), p. 761
- Piran T., 1999, *Phys. Rep.*, 314, 575
- Rau A., McBreen S., Kruehler T., 2009, *GRB Coordinates Network*, 9353, 1
- Razzaque S., 2010, *ApJ*, 724, L109
- Razzaque S., 2013, *Phys. Rev. D*, 88, 103003
- Razzaque S., Dermer C. D., Finke J. D., 2010, *The Open Astronomy Journal*, 3, 150
- Razzaque S., Mészáros P., Zhang B., 2004, *ApJ*, 613, 1072
- Rees M. J., Meszaros P., 1992, *MNRAS*, 258, 41P
- Ronchi M. et al., 2019, arXiv e-prints, arXiv:1909.10531
- Rybicki G. B., Lightman A. P., 1986, *Radiative Processes in Astrophysics*, p. 400
- Sari R., Esin A. A., 2001, *ApJ*, 548, 787
- Sari R., Piran T., Halpern J. P., 1999, *ApJ*, 519, L17
- Sari R., Piran T., Narayan R., 1998, *ApJ*, 497, L17
- Thomas J. K., Moharana R., Razzaque S., 2017, *Phys. Rev. D*, 96, 103004
- van Paradijs J. et al., 1997, *Nature*, 386, 686
- Vietri M., 1997, *ApJ*, 478, L9
- Wang X.-Y., Liu R.-Y., Zhang H.-M., Xi S.-Q., Zhang B., 2019, arXiv e-prints, arXiv:1905.11312
- Wijers R. A. M. J., Galama T. J., 1999, *ApJ*, 523, 177
- Zhang B., Mészáros P., 2001, *ApJ*, 559, 110
- Zhang B., Mészáros P., 2004, *International Journal of Modern Physics A*, 19, 2385
- Zheng W., Deng J., 2010, *Science China Physics, Mechanics, and Astronomy*, 53, 265

APPENDIX

Below we give numerical expressions for the blast-wave evolution parameters, synchrotron parameters and break frequencies, and SSC parameters and break frequencies. These values are described for the adiabatic and radiative blast-waves when they propagate in the constant density medium (ISM) or in a wind-type environment. Here $d_{28} = d_L/10^{28}$ cm and $t_2 = t/100$ s and $\nu_{eV} = \nu/1\text{eV}$.

Adiabatic blast-wave in the constant density medium

$$\Gamma = 124.49 (1+z)^{3/8} n_0^{-1/8} E_{55}^{1/8} t_2^{-3/8} \quad (\text{A-1})$$

$$R = 3.72 \times 10^{17} (1+z)^{-1/4} n_0^{-1/4} E_{55}^{1/4} t_2^{1/4} \text{ cm} \quad (\text{A-2})$$

$$B' = 15.3 (1+z)^{3/8} \epsilon_{B,-1}^{1/2} n_0^{3/8} E_{55}^{1/8} t_2^{-3/8} \text{ G} \quad (\text{A-3})$$

$$\gamma'_m = 2.3 \times 10^4 \left(\frac{p-2}{p-1} \right) (1+z)^{3/8} \epsilon_{e,-1} n_0^{-1/8} E_{55}^{1/8} t_2^{-3/8} \quad (\text{A-4})$$

$$\gamma'_c = 265.33 (1+z)^{-1/8} \epsilon_{B,-1}^{-1} n_0^{-5/8} E_{55}^{-3/8} t_2^{1/8} (1+Y)^{-1} \quad (\text{A-5})$$

$$\gamma'_s = 9.42 \times 10^6 (1+z)^{-3/16} \epsilon_{B,-1}^{-1/4} n_0^{-3/16} \phi_1^{-1/2} E_{55}^{-1/16} t_2^{3/16} (1+Y)^{-1/2} \quad (\text{A-6})$$

$$h\nu_a^f = 1.77 \times 10^{-2} \left[\frac{(p+2)(p-1)}{(3p+2)} \right]^{3/5} (1+z)^{-1/2} \epsilon_{B,-1}^{6/5} n_0^{11/10} E_{55}^{7/10} t_2^{-1/2} (1+Y) \text{ eV} \quad (\text{A-7})$$

$$h\nu_a^s = 2.1 \times 10^{-4} \frac{(p+2)^{3/5} (p-1)^{8/5}}{(3p+2)^{3/5} (p-2)} (1+z)^{-1} \epsilon_{B,-1}^{1/5} \epsilon_{e,-1}^{-1} n_0^{3/5} E_{55}^{1/5} \text{ eV} \quad (\text{A-8})$$

$$h\nu_c = 2.33 (1+z)^{-1/2} \epsilon_{B,-1}^{-3/2} n_0^{-1} E_{55}^{-1/2} t_2^{-1/2} (1+Y)^{-2} \text{ eV} \quad (\text{A-9})$$

$$h\nu_m = 17.3 \left(\frac{p-2}{p-1} \right)^2 (1+z)^{1/2} \epsilon_{B,-1}^{1/2} \epsilon_{e,-1}^2 E_{55}^{1/2} t_2^{-3/2} \text{ keV} \quad (\text{A-10})$$

$$h\nu_s = 2.94 (1+z)^{-5/8} \phi_1^{-1} n_0^{-1/8} E_{55}^{1/8} t_2^{-3/8} (1+Y)^{-1} \text{ GeV} \quad (\text{A-11})$$

The above set of frequencies builds-up the spectral energy distribution for synchrotron emission. For these set of frequencies we also calculate the time when they will appear in the spectrum. We list two most frequent time breaks, t_c and t_m ,

$$t_c = 5.43 \times 10^2 (1+z)^{-1} \epsilon_{B,-1}^{-3} n_0^{-2} E_{55}^{-1} (1+Y)^{-4} \nu_{eV}^{-2} \text{ s} \quad (\text{A-12})$$

$$t_m = 6.69 \times 10^4 \left(\frac{p-2}{p-1} \right)^{4/3} (1+z)^{1/3} \epsilon_{B,-1}^{1/3} \epsilon_{e,-1}^{4/3} E_{55}^{1/3} \nu_{eV}^{-2/3} \text{ s} \quad (\text{A-13})$$

The synchrotron transition time for the fast to slow cooling is calculated for the time when ν_m and ν_c coincides, i.e. $\nu_m(t_0) = \nu_c(t_0)$. The synchrotron and effective inverse-Compton colling times are given by,

$$t_0 = 7.41 \times 10^5 \left(\frac{p-2}{p-1} \right)^2 (1+z) \epsilon_{B,-1}^2 \epsilon_{e,-1}^2 n_0 E_{55} \text{ s} \quad (\text{A-14})$$

$$t_0^{\text{IC}} = 7.41 \times 10^5 \left(\frac{p-2}{p-1} \right)^2 (1+z) \epsilon_{B,-1}^2 \epsilon_{e,-1}^2 n_0 E_{55} (1+Y)^2 \text{ s} \quad (\text{A-15})$$

Now we have listed the set of break frequencies for the SSC component. The SSC component depends on the value of the Y parameter. It has different value during the fast and slow colling, during the fast colling the Compton parameter is $Y = \eta \epsilon_e / \epsilon_B$, where $\eta = 1$, Sari & Esin (2001). For the slow cooling, the Compton parameter is $Y = (\epsilon_e / \epsilon_B)^{1/(4-p)} (t/t_0)^{(2-p)/[2(4-p)]}$. The SSC break frequencies are,

$$h\nu_a^{\text{IC}^f} = 2.41 \left[\frac{(p+2)(p-1)}{3p+2} \right]^{3/5} (1+z)^{-3/4} \epsilon_{B,-1}^{-4/5} n_0^{-3/20} E_{55}^{-1/20} t_2^{-1/4} (1+Y)^{-1} \text{ keV} \quad (\text{A-16})$$

$$h\nu_a^{\text{ICs}} = 0.214 \left[\frac{(p+2)^{3/5}(p-1)^{-2/5}(p-2)}{(3p+2)^{3/5}} \right] (1+z)^{-1/4} \epsilon_{B,-1}^{1/5} \epsilon_{e,-1}^{7/20} n_0^{7/20} E_{55}^{9/20} t_2^{-3/4} \text{ MeV} \quad (\text{A-17})$$

$$h\nu_c^{\text{IC}} = 0.328 (1+z)^{-3/4} \epsilon_{B,-1}^{-7/2} n_0^{-9/4} E_{55}^{-5/4} t_2^{-1/4} (1+Y)^{-4} \text{ MeV} \quad (\text{A-18})$$

$$h\nu_m^{\text{IC}} = 18.1 \left(\frac{p-2}{p-1} \right)^4 (1+z)^{5/4} \epsilon_{B,-1}^{1/2} \epsilon_{e,-1}^4 n_0^{-1/4} E_{55}^{3/4} t_2^{-9/4} \text{ TeV} \quad (\text{A-19})$$

$$h\nu_c^{\text{IC,KN}} = 3.47 (1+z)^{-3/4} \epsilon_{B,-1}^{3/2} n_0^{3/4} E_{55}^{3/4} t_2^{-1/4} (1+Y)^2 \text{ PeV} \quad (\text{A-20})$$

$$h\nu_m^{\text{IC,KN}} = 0.468 \left(\frac{p-1}{p-2} \right)^2 (1+z)^{-7/4} \epsilon_{B,-1}^{-1/2} \epsilon_{e,-1}^{-2} n_0^{-1/4} E_{55}^{-1/4} t_2^{3/4} \text{ TeV} \quad (\text{A-21})$$

The break times for minimum and cooling frequencies are defined as,

$$t_c^{\text{IC}} = 1.16 \times 10^{24} (1+z)^{-3} \epsilon_{B,-1}^{-14} n_0^{-9} E_{55}^{-5} (1+Y)^{-16} \nu_{\text{eV}}^{-4} \text{ s} \quad (\text{A-22})$$

$$t_m^{\text{IC}} = 7.87 \times 10^7 \left(\frac{p-2}{p-1} \right)^{16/9} (1+z)^{5/9} \epsilon_{B,-1}^{2/9} \epsilon_{e,-1}^{16/9} n_0^{-1/9} E_{55}^{1/3} \nu_{\text{eV}}^{-4/9} \text{ s} \quad (\text{A-23})$$

The maximum flux values for the synchrotron and SSC emission are,

$$f_{\nu,\text{max}} = 8.22 (1+z)^{-1} \epsilon_{B,-1}^{1/2} n_0^{1/2} E_{55} d_{28}^{-2} \text{ Jy}. \quad (\text{A-24})$$

$$f_{\nu,\text{max}}^{\text{IC}} = 5.42 \times 10^{-6} (1+z)^{-5/4} \epsilon_{B,-1}^{1/2} n_0^{5/4} E_{55}^{5/4} t_2^{1/4} d_{28}^{-2} \text{ Jy}. \quad (\text{A-25})$$

Adiabatic blast-wave into the wind medium

The parameters have the same physical meaning as for the expression defined above.

$$\Gamma = 78.25 (1+z)^{1/4} A_\star^{-1/4} E_{55}^{1/4} t_2^{-1/4}. \quad (\text{A-26})$$

$$R = 1.47 \times 10^{17} (1+z)^{-1/2} A_\star^{-1/2} E_{55}^{1/2} t_2^{1/2} \text{ cm}. \quad (\text{A-27})$$

$$B' = 35.96 (1+z)^{3/4} \epsilon_{B,-1}^{1/2} A_\star^{3/4} E_{55}^{-1/4} t_2^{-3/4} \text{ G}. \quad (\text{A-28})$$

$$\gamma'_m = 1.44 \times 10^4 \left(\frac{p-2}{p-1} \right) (1+z)^{1/4} \epsilon_{e,-1} A_\star^{-1/4} E_{55}^{1/4} t_2^{-1/4} \quad (\text{A-29})$$

$$\gamma'_c = 76.41 (1+z)^{-3/4} \epsilon_{B,-1}^{-1} A_\star^{-5/4} E_{55}^{1/4} t_2^{3/4} (1+Y)^{-1} \quad (\text{A-30})$$

$$\gamma'_s = 6.15 \times 10^6 (1+z)^{-3/8} \epsilon_{B,-1}^{-1/4} \phi_1^{-1/2} A_\star^{-3/8} E_{55}^{1/8} t_2^{3/8} (1+Y)^{-1/2} \quad (\text{A-31})$$

$$h\nu_a^{\text{fast}} = 0.15 \left[\frac{(p-1)(p+2)}{(3p+2)} \right]^{3/5} (1+z)^{3/5} \epsilon_{B,-1}^{6/5} A_\star^{11/5} E_{55}^{-2/5} t_2^{-8/5} (1+Y) \text{ eV}. \quad (\text{A-32})$$

$$h\nu_a^{\text{slow}} = 0.00081 \frac{(p-1)^{8/5}(p+2)^{3/5}}{(3p+2)^{3/5}(p-2)} (1+z)^{-2/5} \epsilon_{B,-1}^{1/5} \epsilon_{e,-1}^{-1} A_\star^{6/5} E_{55}^{-2/5} t_2^{-3/5} \text{ eV}. \quad (\text{A-33})$$

$$h\nu_c = 0.29 (1+z)^{-3/2} \epsilon_{B,-1}^{-3/2} A_\star^{-2} E_{55}^{1/2} t_2^{1/2} (1+Y)^{-2} \text{ eV}. \quad (\text{A-34})$$

$$h\nu_m = 1.01 \times 10^4 \left(\frac{p-2}{p-1} \right)^2 (1+z)^{1/2} \epsilon_{B,-1}^{1/2} \epsilon_{e,-1}^2 E_{55}^{1/2} t_2^{-3/2} \text{ eV}. \quad (\text{A-35})$$

$$h\nu_s = 1.85 (1+z)^{-3/4} \phi_1^{-1} A_\star^{-1/4} E_{55}^{1/4} t_2^{-1/4} (1+Y)^{-1} \text{ GeV}. \quad (\text{A-36})$$

$$t_c = 1.21 \times 10^3 (1+z)^3 \epsilon_{B,-1}^3 A_\star^4 E_{55}^{-1} (1+Y)^4 \nu_{\text{eV}}^2 \text{ s} \quad (\text{A-37})$$

$$t_m = 4.67 \times 10^4 \left(\frac{p-2}{p-1} \right)^{4/3} (1+z)^{1/3} \epsilon_{B,-1}^{1/3} \epsilon_{e,-1}^{4/3} E_{55}^{1/3} \nu_{\text{eV}}^{-2/3} \text{ s} \quad (\text{A-38})$$

$$t_0 = 1.88 \times 10^4 \left(\frac{p-2}{p-1} \right) (1+z) \epsilon_{B,-1} \epsilon_{e,-1} A_\star \text{ s} \quad (\text{A-39})$$

$$t_0^{\text{IC}} = 1.88 \times 10^4 \left(\frac{p-2}{p-1} \right) (1+z) \epsilon_{B,-1} \epsilon_{e,-1} A_\star (1+Y) \text{ s} \quad (\text{A-40})$$

The Compton factor during the fast cooling don't change and for slow cooling its value is $Y = (\epsilon_e/\epsilon_B)^{1/(4-p)} (t/t_0)^{(2-p)/4-p}$.

$$h\nu_a^{\text{IC}^f} = 1770.04 \left[\frac{(p+2)(p-1)}{3p+2} \right]^{3/5} (1+z)^{9/10} \epsilon_{B,-1}^{-4/5} A_\star^{-3/10} E_{55}^{1/10} t_2^{-1/10} (1+Y)^{-1} \text{ eV}. \quad (\text{A-41})$$

$$h\nu_a^{\text{IC}^s} = 3.33 \times 10^5 \frac{(p-2)(p+2)^{3/5}}{(3p+2)^{3/5}(p-1)^{2/5}} (1+z)^{1/10} \epsilon_{B,-1}^{1/5} \epsilon_{e,-1} A_\star^{7/10} E_{55}^{1/10} t_2^{-11/10} \text{ eV}. \quad (\text{A-42})$$

$$h\nu_c^{\text{IC}} = 3.34 \times 10^3 (1+z)^{-3} \epsilon_{B,-1}^{-7/2} A_\star^{-9/2} E_{55} t_2^2 (1+Y)^{-4} \text{ eV}. \quad (\text{A-43})$$

$$h\nu_m^{\text{IC}} = 4.17 \left(\frac{p-2}{p-1} \right)^4 (1+z) \epsilon_{B,-1}^{1/2} \epsilon_{e,-1}^4 E_{55} A_\star^{-1/2} t_2^{-2} \text{ TeV}. \quad (\text{A-44})$$

$$h\nu_c^{\text{IC,KN}} = 11 \epsilon_{B,-1}^{3/2} A_\star^{3/2} t_2^{-1} (1+Y)^2 \text{ PeV} \quad (\text{A-45})$$

$$h\nu_m^{\text{IC,KN}} = 0.32 \left(\frac{p-1}{p-2} \right)^2 (1+z)^{-2} \epsilon_{B,-1}^{-1/2} \epsilon_{e,-1}^{-2} A_\star^{-1/2} t_2 \text{ TeV} \quad (\text{A-46})$$

$$t_c^{\text{IC}} = 1.1 \times 10^{-7} (1+z)^{3/2} \epsilon_{B,-1}^{7/4} A_\star^{9/4} E_{55}^{-1/2} (1+Y)^2 \nu_{\text{eV}}^{1/2} \text{ s}. \quad (\text{A-47})$$

$$t_m^{\text{IC}} = 2.04 \times 10^8 \left(\frac{p-2}{p-1} \right)^2 (1+z)^{1/2} \epsilon_{B,-1}^{1/4} \epsilon_{e,-1}^2 E_{55}^{1/2} \nu_{\text{eV}}^{-1/2} \text{ s} \quad (\text{A-48})$$

$$f_{\nu,\text{max}} = 10.44 (1+z)^{-1/2} \epsilon_{B,-1}^{1/2} A_\star E_{55}^{1/2} t_2^{-1/2} d_{28}^{-2} \text{ Jy}. \quad (\text{A-49})$$

$$f_{\nu,\text{max}}^{\text{IC}} = 3.81 \times 10^{-5} \epsilon_{B,-1}^{1/2} A_\star^{5/2} t_2^{-1} d_{28}^{-2} \text{ Jy}. \quad (\text{A-50})$$

Radiative blast-wave into the constant density medium

$$\Gamma = 85.73 (1+z)^{3/7} n_0^{-1/7} \Gamma_{2.5}^{-1/7} E_{55}^{1/7} t_2^{-3/7}. \quad (\text{A-51})$$

$$R = 3.1 \times 10^{17} (1+z)^{-1/7} n_0^{-2/7} \Gamma_{2.5}^{-2/7} E_{55}^{2/7} t_2^{1/7} \text{ cm}. \quad (\text{A-52})$$

$$B' = 10.54 (1+z)^{3/7} \epsilon_{B,-1}^{1/2} n_0^{5/14} \Gamma_{2.5}^{-1/7} E_{55}^{1/7} t_2^{-3/7} \text{ G}. \quad (\text{A-53})$$

$$\gamma'_m = 1.6 \times 10^4 \left(\frac{p-2}{p-1} \right) (1+z)^{3/7} \epsilon_{e,-1} n_0^{-1/7} \Gamma_{2.5}^{-1/7} E_{55}^{1/7} t_2^{-3/7}. \quad (\text{A-54})$$

$$\gamma'_c = 812.42 (1+z)^{-2/7} \epsilon_{B,-1}^{-1} n_0^{-4/7} \Gamma_{2.5}^{3/7} E_{55}^{-3/7} t_2^{2/7} (1+Y)^{-1}. \quad (\text{A-55})$$

$$\gamma'_s = 1.14 \times 10^7 (1+z)^{-3/14} \epsilon_{B,-1}^{-1/4} n_0^{-5/28} \phi_1^{-1/2} \Gamma_{2.5}^{1/14} E_{55}^{-1/14} t_2^{3/14} (1+Y)^{-1/2} \quad (\text{A-56})$$

$$h\nu_a^{\text{fast}} = 3.1 \times 10^{-3} \left[\frac{(p+2)(p-1)}{3p+2} \right]^{3/5} (1+z)^{-1/5} \epsilon_{B,-1}^{6/5} n_0 \Gamma_{2.5}^{-4/5} E_{55}^{4/5} t_2^{-4/5} (1+Y) \text{ eV}. \quad (\text{A-57})$$

$$h\nu_a^{\text{slow}} = 1.5 \times 10^{-4} \frac{(p+2)^{3/5} (p-1)^{8/5}}{(p-2)(3p+2)^{3/5}} (1+z)^{-32/35} \epsilon_{B,-1}^{1/5} \epsilon_{e,-1}^{-1} n_0^{4/7} \Gamma_{2.5}^{-8/35} E_{55}^{8/35} t_2^{-3/35} \text{ eV}. \quad (\text{A-58})$$

$$h\nu_c = 10.38 (1+z)^{-5/7} \epsilon_{B,-1}^{-3/2} n_0^{-13/14} \Gamma_{2.5}^{4/7} E_{55}^{-4/7} t_2^{-2/7} (1+Y)^{-2} \text{ eV}. \quad (\text{A-59})$$

$$h\nu_m = 4.1 \left(\frac{p-2}{p-1} \right)^2 (1+z)^{5/7} \epsilon_{B,-1}^{1/2} \epsilon_{e,-1}^2 n_0^{-1/14} \Gamma_{2.5}^{-4/7} E_{55}^{4/7} t_2^{-12/7} \text{ keV}. \quad (\text{A-60})$$

$$h\nu_s = 2.03 (1+z)^{-4/7} \phi_1^{-1} n_0^{-1/7} \Gamma_{2.5}^{-1/7} E_{55}^{1/7} t_2^{-3/7} (1+Y)^{-1} \text{ GeV}. \quad (\text{A-61})$$

$$t_c = 3.6 \times 10^5 (1+z)^{-5/2} \epsilon_{B,-1}^{-21/4} n_0^{-13/4} \Gamma_{2.5}^2 E_{55}^{-2} (1+Y)^{-7} \nu_{\text{eV}}^{-7/2} \text{ s}. \quad (\text{A-62})$$

$$t_m = 1.28 \times 10^4 \left(\frac{p-2}{p-1} \right)^{7/6} (1+z)^{5/12} \epsilon_{B,-1}^{7/24} \epsilon_{e,-1}^{7/6} n_0^{-1/24} \Gamma_{2.5}^{-1/3} E_{55}^{1/3} \nu_{\text{eV}}^{-7/12} \text{ s}. \quad (\text{A-63})$$

$$t_0 = 6.34 \times 10^3 \left(\frac{p-2}{p-1} \right)^{7/5} (1+z) \epsilon_{B,-1}^{7/5} \epsilon_{e,-1}^{7/5} n_0^{3/5} \Gamma_{2.5}^{-4/5} E_{55}^{4/5} \text{ s}. \quad (\text{A-64})$$

$$t_0^{\text{IC}} = 6.34 \times 10^3 \left(\frac{p-2}{p-1} \right)^{7/5} (1+z) \epsilon_{B,-1}^{7/5} \epsilon_{e,-1}^{7/5} n_0^{3/5} \Gamma_{2.5}^{-4/5} E_{55}^{4/5} (1+Y)^{7/5} \text{ s}. \quad (\text{A-65})$$

The Compton parameter for the slow-cooling phase is $Y = (\epsilon_e/\epsilon_B)^{1/(4-p)} (t/t_0)^{5(2-p)/[7(4-p)]}$.

$$h\nu_a^{\text{ICf}} = 4.05 \left[\frac{(p+2)(p-1)}{3p+2} \right]^{3/5} (1+z)^{-27/35} \epsilon_{B,-1}^{-4/5} n_0^{-1/7} \Gamma_{2.5}^{2/35} E_{55}^{-2/35} t_2^{-8/35} (1+Y)^{-1} \text{ keV}. \quad (\text{A-66})$$

$$h\nu_a^{\text{ICs}} = 79.1 \left[\frac{(p+2)}{3p+2} \right]^{3/5} \frac{(p-2)}{(p-1)^{2/5}} (1+z)^{-2/35} \epsilon_{B,-1}^{1/5} \epsilon_{e,-1} n_0^{2/7} \Gamma_{2.5}^{-18/35} E_{55}^{18/35} t_2^{-33/35} \text{ keV}. \quad (\text{A-67})$$

$$h\nu_c^{\text{IC}} = 13.7 (1+z)^{-9/7} \epsilon_{B,-1}^{-7/2} n_0^{-29/14} \Gamma_{2.5}^{10/7} E_{55}^{-10/7} t_2^{2/7} (1+Y)^{-4} \text{ MeV}. \quad (\text{A-68})$$

$$h\nu_m^{\text{IC}} = 1.93 \left(\frac{p-2}{p-1} \right)^4 (1+z)^{11/7} \epsilon_{B,-1}^{1/2} \epsilon_{e,-1}^4 n_0^{-5/14} \Gamma_{2.5}^{-6/7} E_{55}^{6/7} t_2^{-18/7} \text{ TeV}. \quad (\text{A-69})$$

$$h\nu_c^{\text{IC,KN}} = 0.37 (1+z)^{-3/7} \epsilon_{B,-1}^{3/2} n_0^{9/14} \Gamma_{2.5}^{-6/7} E_{55}^{6/7} t_2^{-4/7} (1+Y)^2 \text{ PeV}. \quad (\text{A-70})$$

$$h\nu_m^{\text{IC,KN}} = 0.94 \left(\frac{p-1}{p-2} \right)^2 (1+z)^{-13/7} \epsilon_{B,-1}^{-1/2} \epsilon_{e,-1}^{-2} n_0^{-3/14} \Gamma_{2.5}^{2/7} E_{55}^{-2/7} t_2^{6/7} \text{ TeV}. \quad (\text{A-71})$$

$$t_c^{\text{IC}} = 1.05 \times 10^{-23} (1+z)^{9/2} \epsilon_{B,-1}^{49/4} n_0^{29/4} \Gamma_{2.5}^{-5} E_{55}^5 (1+Y)^{14} \nu_{\text{eV}}^{7/2} \text{ s}. \quad (\text{A-72})$$

$$t_m^{\text{IC}} = 6.1 \times 10^6 \left(\frac{p-2}{p-1} \right)^{14/9} (1+z)^{11/18} \epsilon_{B,-1}^{7/36} \epsilon_{e,-1}^{14/9} n_0^{-5/36} \Gamma_{2.5}^{-1/3} E_{55}^{1/3} \nu_{\text{eV}}^{-7/18} \text{ s}, \quad (\text{A-73})$$

$$f_{\nu,\text{max}} = 2.22 (1+z)^{-4/7} \epsilon_{B,-1}^{1/2} n_0^{5/14} \Gamma_{2.5}^{-8/7} E_{55}^{8/7} t_2^{-3/7} d_{28}^{-2} \text{ Jy}. \quad (\text{A-74})$$

$$f_{\nu,\text{max}}^{\text{IC}} = 1.22 \times 10^{-6} (1+z)^{-5/7} \epsilon_{B,-1}^{1/2} n_0^{15/14} \Gamma_{2.5}^{-10/7} E_{55}^{10/7} t_2^{-2/7} \text{ Jy}. \quad (\text{A-75})$$

7.1 Radiative blast-wave into the wind medium

$$\Gamma = 40.77 (1+z)^{1/3} A_\star^{-1/3} \Gamma_{2.5}^{-1/3} E_{55}^{1/3} t_2^{-1/3}. \quad (\text{A-76})$$

$$R = 6.98 \times 10^{16} (1+z)^{-1/3} A_\star^{-2/3} \Gamma_{2.5}^{-2/3} E_{55}^{2/3} t_2^{1/3} \text{ cm}. \quad (\text{A-77})$$

$$B' = 39.44 (1+z)^{2/3} \epsilon_{B,-1}^{1/2} A_{\star}^{5/6} \Gamma_{2.5}^{1/3} E_{55}^{-1/3} t_2^{-2/3} G. \quad (\text{A-78})$$

$$\gamma'_m = 7.5 \times 10^3 \left(\frac{p-2}{p-1} \right) (1+z)^{1/3} \epsilon_{e,-1} A_{\star}^{-1/3} \Gamma_{2.5}^{-1/3} E_{55}^{1/3} t_2^{-1/3}. \quad (\text{A-79})$$

$$\gamma'_c = 122 (1+z)^{-2/3} \epsilon_{B,-1}^{-1} A_{\star}^{-4/3} \Gamma_{2.5}^{-1/3} E_{55}^{1/3} t_2^{2/3} (1+Y)^{-1}. \quad (\text{A-80})$$

$$\gamma'_s = 5.87 \times 10^6 (1+z)^{-1/3} \epsilon_{B,-1}^{-1/4} A_{\star}^{-5/12} \phi_1^{-1/2} \Gamma_{2.5}^{-1/6} E_{55}^{1/6} t_2^{1/3} (1+Y)^{-1/2}. \quad (\text{A-81})$$

$$h\nu_a^{\text{fast}} = 0.08 \left[\frac{(p+2)(p-1)}{3p+2} \right]^{3/5} (1+z)^{7/15} \epsilon_{B,-1}^{6/5} A_{\star}^{7/3} \Gamma_{2.5}^{8/15} E_{55}^{-8/15} t_2^{-22/15} (1+Y) \text{ eV} \quad (\text{A-82})$$

$$h\nu_a^{\text{slow}} = 0.0013 \left(\frac{p+2}{3p+2} \right)^{3/5} \frac{(p-1)^{8/5}}{p-2} (1+z)^{-8/15} \epsilon_{e,-1}^{1/5} \epsilon_{B,-1}^{4/3} \Gamma_{2.5}^{8/15} E_{55}^{-8/15} t_2^{-7/15} \text{ eV}. \quad (\text{A-83})$$

$$h\nu_c = 0.41 (1+z)^{-4/3} \epsilon_{B,-1}^{-3/2} A_{\star}^{-13/6} \Gamma_{2.5}^{-2/3} E_{55}^{2/3} t_2^{1/3} (1+Y)^{-2} \text{ eV}. \quad (\text{A-84})$$

$$h\nu_m = 1.57 \left(\frac{p-2}{p-1} \right)^2 (1+z)^{2/3} \epsilon_{B,-1}^{1/2} \epsilon_{e,-1}^2 A_{\star}^{-1/6} \Gamma_{2.5}^{-2/3} E_{55}^{2/3} t_2^{-5/3} \text{ keV}. \quad (\text{A-85})$$

$$h\nu_s = 9.63 \times 10^8 (1+z)^{-2/3} \phi_1^{-1} A_{\star}^{-1/3} \Gamma_{2.5}^{-1/3} E_{55}^{1/3} t_2^{-1/3} (1+Y)^{-1} \text{ eV}. \quad (\text{A-86})$$

$$t_c = 1.45 \times 10^3 (1+z)^4 \epsilon_{B,-1}^{9/2} A_{\star}^{13/2} \Gamma_{2.5}^2 E_{55}^{-2} (1+Y)^6 \nu^3 \text{ s}. \quad (\text{A-87})$$

$$t_m = 8.3 \times 10^3 \left(\frac{p-2}{p-1} \right)^{6/5} (1+z)^{2/5} \epsilon_{B,-1}^{3/10} \epsilon_{e,-1}^{6/5} A_{\star}^{-1/10} \Gamma_{2.5}^{-2/5} E_{55}^{2/5} \nu^{-3/5} \text{ s} \quad (\text{A-88})$$

$$t_0 = 6.1 \times 10^3 \left(\frac{p-2}{p-1} \right) (1+z) \epsilon_{B,-1} \epsilon_{e,-1} A_{\star} (1+Y) \text{ s}. \quad (\text{A-89})$$

$$t_0^{\text{IC}} = 6.1 \times 10^3 \left(\frac{p-2}{p-1} \right) (1+z) \epsilon_{B,-1} \epsilon_{e,-1} A_{\star} (1+Y) \text{ s}. \quad (\text{A-90})$$

The Compton parameter during the slow phase is $Y = (\epsilon_e/\epsilon_B)^{1/(4-p)} (t/t_0)^{(2-p)/4-p}$.

$$h\nu_a^{\text{ICf}} = 2.43 \left(\frac{(p+2)(p-1)}{3p+2} \right)^{3/5} (1+z)^{-13/15} \epsilon_{B,-1}^{-4/5} A_{\star}^{-1/3} \Gamma_{2.5}^{-2/15} E_{55}^{2/15} t_2^{-2/15} (1+Y)^{-1} \text{ keV}. \quad (\text{A-91})$$

$$h\nu_a^{\text{ICs}} = 0.15 \left(\frac{p+2}{3p+2} \right)^{3/5} \frac{(p-2)}{(p-1)^{2/5}} (1+z)^{2/15} \epsilon_{B,-1}^{1/5} \epsilon_{e,-1} A_{\star}^{2/3} \Gamma_{2.5}^{-2/15} E_{55}^{2/15} t_2^{-17/15} \text{ MeV}. \quad (\text{A-92})$$

$$h\nu_c^{\text{IC}} = 12.4 (1+z)^{-8/3} \epsilon_{B,-1}^{-7/2} A_{\star}^{-29/6} \Gamma_{2.5}^{-4/3} E_{55}^{4/3} t_2^{5/3} (1+Y)^{-4} \text{ keV}. \quad (\text{A-93})$$

$$h\nu_m^{\text{IC}} = 0.176 \left(\frac{p-2}{p-1} \right)^4 (1+z)^{4/3} \epsilon_{B,-1}^{1/2} \epsilon_{e,-1}^4 A_{\star}^{-5/6} \Gamma_{2.5}^{-4/3} E_{55}^{4/3} t_2^{-7/3} \text{ TeV}. \quad (\text{A-94})$$

$$h\nu_c^{\text{IC,KN}} = 2.12 A_{\star}^{3/2} \epsilon_{B,-1}^{3/2} t_2^{-1} (1+Y)^2 \text{ PeV}. \quad (\text{A-95})$$

$$h\nu_m^{\text{IC,KN}} = 0.553 \left(\frac{p-1}{p-2} \right)^2 (1+z)^{-2} \epsilon_{B,-1}^{-1/2} \epsilon_{e,-1}^{-2} A_{\star}^{-1/2} t_2 \text{ TeV}. \quad (\text{A-96})$$

$$t_c^{\text{IC}} = 1.39 (1+z)^{8/5} \epsilon_{B,-1}^{21/10} A_{\star}^{29/10} \Gamma_{2.5}^{4/5} E_{55}^{-4/5} (1+Y)^{12/5} \nu_e^{3/5} \text{ s}. \quad (\text{A-97})$$

$$t_m^{\text{IC}} = 6.61 \times 10^6 \left(\frac{p-2}{p-1} \right)^{12/7} (1+z)^{4/7} \epsilon_{B,-1}^{3/14} \epsilon_{e,-1}^{12/7} A_{\star}^{-5/14} \Gamma_{2.5}^{-4/7} E_{55}^{4/7} \nu_e^{-3/7} \text{ s}. \quad (\text{A-98})$$

$$f\nu_{\text{max}} = 2.83 (1+z)^{-1/3} \epsilon_{B,-1}^{1/2} A_{\star}^{5/6} \Gamma_{2.5}^{-2/3} E_{55}^{2/3} t_2^{-2/3} d_{28}^{-2} \text{ Jy}. \quad (\text{A-99})$$

$$f\nu_{\text{max}}^{\text{IC}} = 2.17 \times 10^{-5} \epsilon_{B,-1}^{1/2} A_{\star}^{5/2} t_2^{-1} d_{28}^{-2} \text{ Jy}. \quad (\text{A-100})$$

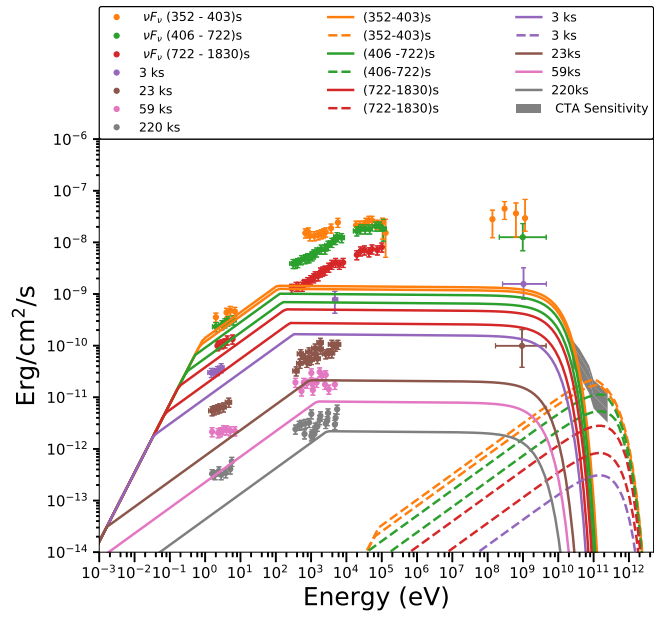


Figure 4. The contribution of the second component is shown for GRB 130427A. This component is mainly important for the late radio emission observed from this GRB.